

Universal Surface-Defect Passivant for Perovskite Solar Cells Based on N-Phenylglycine for Improved Photovoltaic Performance and Stability

Dingbo Zhang, Xin Liu, Yuanzheng Chen[✉], Yudong Xia, Yongliang Tang, Hongyan Wang, and Yuxiang Ni^{✉*}

School of Physical Science and Technology, Southwest Jiaotong University, Chengdu 610031, China



(Received 30 July 2021; revised 8 December 2021; accepted 21 January 2022; published 14 February 2022)

In this work, we use N-phenylglycine (NPG) molecules as a universal passivant for all typical surface defects of perovskite to improve the photovoltaic performance and stability of perovskite. Our results show that NPG molecules can passivate the organic cation vacancy, I⁻ vacancy, Pb²⁺ vacancy, and Pb-I antisite surface defects of perovskite, through either coordinate and/or hydrogen bonding, or the van der Waals interaction. More interestingly, after the Pb²⁺ vacancy on the perovskite surface is passivated by NPG, a transition from metallic to semiconducting properties occurs. The perovskite solar cells (PSCs) passivated by NPG have a high power conversion efficiency (PCE) of 21.16% and retain 91% of the initial efficiency after 700 h in humid air, compared with PSCs without passivation (PCE of 18.29% and maintained efficiency of 75%). Our study proposes one general surface-defect passivant for PSCs that significantly boosts photovoltaic performance and stability.

DOI: 10.1103/PhysRevApplied.17.024039

I. INTRODUCTION

Metal halide perovskite is regarded as an ideal light absorber for solar cells [1] owing to its tunable band gap [2], low exciton binding energy [3], high charge transport mobility [4], high absorption coefficient [5,6], etc. To date, the power conversion efficiency (PCE) of lab-scale perovskite solar cells (PSCs) has already surpassed 25% [7,8], making PSCs the front runner among the emerging solar cells [9]. Usually, the prepared perovskite films are polycrystalline with various defects and charge traps in the vicinity of the grain boundaries and surfaces [10,11]. The defects and charge traps act as recombination centers that hinder the separation of photogenerated electron-hole pairs, which unfortunately shortens the lifetime of charge carriers [12]. More importantly, external factors (moisture, heat, oxygen, etc.) can accelerate ion migration in the defected perovskite, which causes the collapse of the lattice and ultimately undermines the photovoltaic performance [13]. Therefore, passivating the defects of perovskite is imperative to improve the efficiency and stability of PSCs.

In recent years, progress has been made in the passivation of perovskite, which has largely improved the performance and stability of PSCs [10]. The typical surface defects of organic perovskite, including organic cation vacancy, I⁻ vacancy, Pb²⁺ vacancy, and Pb-I antisite surface defects [14], can be passivated by Lewis acid [15], trimethylolpropane triacrylate [16], π -conjugated molecules

[17], and theophylline [18], respectively. The related passivation mechanism for each defect is different, including molecular replacement, strain-regulating crystallization, formation of chemical bonding, and charge interaction. Therefore, it is difficult to achieve the passivation of perovskite with one single passivant, which would otherwise largely facilitate the passivation treatment and improve the overall PSC efficiency.

To make progress, in this work, we propose N-phenylglycine (NPG) as a universal passivant to passivate all typical surface defects of $(\text{FAPbI}_3)_x(\text{MAPbBr}_3)_{1-x}$ ($x = 0.92$) (FA: formamidinium, MA: methylammonium). The abundant chemical groups (C-H, N-H, O-H, C=O, and benzene ring) in NPG molecules provide multiple ways to interact with and passivate various surface defects. Furthermore, NPG has many inherent advantages, such as ease of synthesis, a well-defined structure, and good moisture tolerance, etc. [16]. Combining experiments and first-principles calculations, we explore the quality of perovskite films passivated by NPG, and reveal the passivation mechanisms of NPG for different surface defects of perovskite. The corresponding PSCs are prepared and the measured PCE of the PSCs is significantly larger than that of the pristine devices. The stability of the PSCs is also improved, with 9% efficiency loss after 700 h in humid air.

II. RESULTS AND DISCUSSIONS

A. The defected structures of pristine and NPG-passivated perovskite

In high-quality perovskite polycrystalline films, the surface defects of perovskite have an obvious influence on the

*yuxiang.ni@swjtu.edu.cn

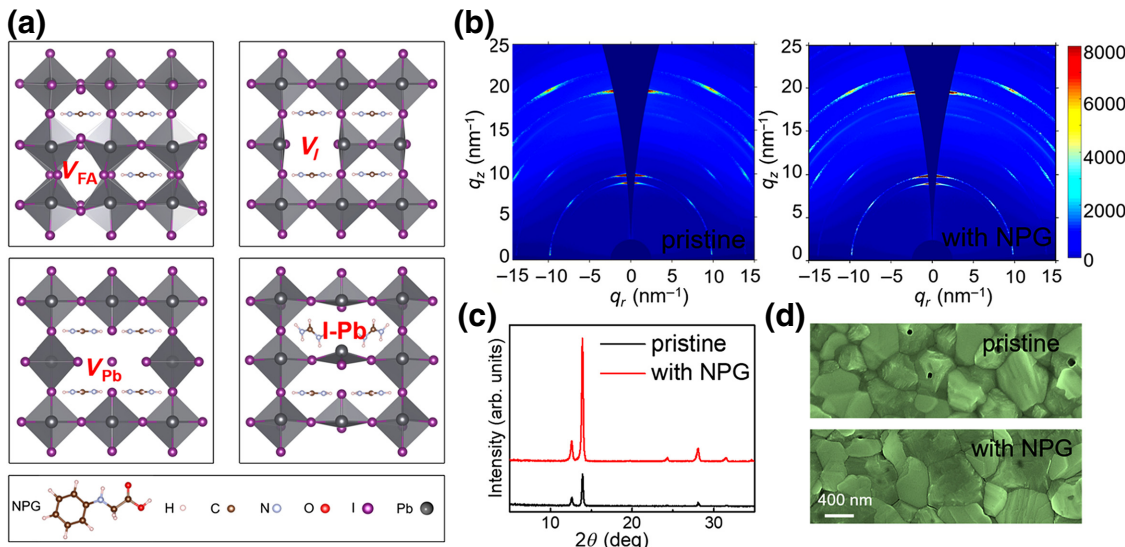


FIG. 1. The structural identification. (a) Atomistic model of the defects on the perovskite surface (top view) and the structure of NPG molecule. The defects include organic cation vacancy (V_{FA}), I⁻ vacancy (V_I), Pb²⁺ vacancy (V_{Pb}), and Pb-I antisite defect ($I-Pb$). (b) GIWAXS data of pristine and NPG-passivated perovskite films, and the intensity distribution is identified by the color legend. (c) XRD patterns of pristine and NPG-passivated perovskite films. (d) SEM micrographs of pristine and NPG-passivated perovskite films.

structural stability compared with interior defects [19]. We first identify the structures of the defected perovskite by using density functional theory (DFT) calculations [20]. The Vienna *ab initio* simulation package (VASP) code is used in the calculations [21,22]. The perovskite structure is simplified as the FAPbI₃ perovskite, which is the major component of perovskite. The optimized structures of the defected perovskite and NPG molecule are presented in Fig. 1(a). The geometry structure and band structure of FAPbI₃ primitive cell are also obtained (see Fig. S1 within the Supplemental Material [23]), and these comply well with previous reports [24]. The negative formation energies (E_f) of the FA vacancy (V_{FA}), I⁻ vacancy (V_I), Pb²⁺ vacancy (V_{Pb}), and Pb-I antisite defect ($I-Pb$) indicate that all these typical surface defects exist in perovskite. Moreover, the negative binding energies between NPG and the perovskite surface defects, as listed Table I, suggest that NPG can effectively bind to the defected perovskite surface.

We adopt NPG to passivate the perovskite surface defects, and then compare the quality of pristine and

NPG-passivated perovskite films by grazing-incidence wide-angle x-ray scattering (GIWAXS), x-ray diffraction (XRD) analysis, and scanning electron microscopy (SEM). Details of the sample preparation and characterizations can be found in the Supplemental Material [23]. As illustrated in Fig. 1(b), the GIWAXS patterns of pristine films show sporadic Bragg spots, indicating an anisotropic orientation distribution of the crystallite [25]. The samples treated with NPG show higher diffraction intensity along the (110) ring ($|q| = 10 \text{ nm}^{-1}$, where q is the scattering vector.) and (220) ring ($|q| = 20 \text{ nm}^{-1}$) that belong to the perovskite phase, which indicates better crystallinity compared with the pristine films. The one-dimensional GIWAXS figure also corroborates this phenomenon, as demonstrated in Fig. S2 in the Supplemental Material [23]. Figure 1(c) shows that the XRD peak positions of the pristine and NPG-passivated perovskite remain unaltered. However, there is a substantial increase in the peak intensity of the passivated perovskite, suggesting the enhancement of its crystallinity. Although the cross-section SEM images (see Fig. S3 in the Supplemental Material [23]) show little difference in thickness between the pristine films and the NPG-passivated films, the SEM micrographs [see Fig. 1(d)] clearly show a more uniform morphology and larger grain size of the passivated films compared with the pristine ones. The defect state density of the perovskite film after the passivation is smaller than that of the pristine one (see the trap density of states in Fig. S4 in the Supplemental Material [23]), indicating that NPG can effectively passivate the various defects on the surface of the perovskite. More notably, by combining the trap density of states (tDOS) and the surface-defect formation energy, one can see that the

TABLE I. The surface-defect formation energies (E_f) and the binding energies (E_b) between NPG molecule and each surface defect in the perovskite.

Defect type	E_f (eV)	Type of contact	E_b (eV)
V_{FA}	-1.59	V_{FA} -NPG	-2.53
V_I	-0.86	V_I -NPG	-2.77
V_{Pb}	-3.35	V_{Pb} -NPG	-2.36
Pb-I antisite	-3.02	Pb-I-antisite-NPG	-1.11

vacancy defects are not only shallow level defects, but are also passivated by NPG. These characterizations clearly show that the quality of the perovskite films is improved by the NPG passivation.

The residual PbI_2 peak appears at $|q| = 0.88\text{--}0.94 \text{ nm}^{-1}$ of the GIWAXS patterns and 12.72° of the XRD patterns for the pristine films. The residual PbI_2 helps to increase the efficiency of the corresponding devices, but it also causes the instability of the perovskite structure [13]. The results of the XRD patterns suggest that the ratio of PbI_2 to perovskite is reduced with the addition of NPG, indicating that the NPG molecules interact with PbI_2 and reduce its quantity, and therefore the film crystallinity is enhanced.

B. Interaction mechanism between perovskite films and NPG

To understand the passivation mechanism of NPG for perovskite surface defects, we analyze the interface structures [see Fig. 2(a)]. As NPG passivates V_{FA} on the perovskite surface, the hydrogen atoms in H-N and H-O of NPG form hydrogen bonds with different I atoms near the FA vacancy site. The oxygen atoms in O=C bond with the surface Pb atoms near the FA vacancy site. When NPG interacts with V_{I} on the perovskite surface, the Pb atom with a dangling bond in the vicinity of the I vacancy forms hydrogen bonds and coordinate bonds with hydrogen in H-N and oxygen in C=O of NPG, respectively. The details of bond lengths can be found Table S1 in the Supplemental Material [23]. The bonding always inhibits the drift

of isolated ions or clusters in perovskite, and induces the formation of an interfacial dipole and carrier channel. It can also promote the charge transfer from perovskite to the molecules and the hydrophobicity of the perovskite film.

On the other hand, the pivotal mechanism for interaction between NPG and the other two defects (V_{Pb} and Pb-I) is based on the van der Waals force, which can create many interesting optical and electronic properties, such as enhanced light absorption and effective hole-electron separation. Notably, the detailed passivating behaviors of NPG on the two defects are different. For V_{Pb} surface defects, the H-N, H-O, and benzene ring of NPG interact with different I atoms near the Pb vacancy site, respectively, and then the defect is passivated. For Pb-I antisite surface defects, the formation of the hydrogen bond between NPG (H-N) and the perovskite surface (I) confines the position of C=O (in NPG) in the vicinity of the Pb-I antisite, which induces the formation of a van der Waals interaction between C=O and Pb-I antisite. Consequently, NPG stabilizes the structures of perovskite and increases the photoelectric performance of perovskite, as depicted in Fig. 2(b).

C. The effects of NPG on optoelectronic properties of perovskite films

In this section, we focus on the impact of NPG on the optoelectronic properties of perovskite films through computational simulation and experimental characterization. According to Fig. 3(a), an obvious band-edge shift can be observed for both the highest occupied molecular orbital (HOMO) and the lowest unoccupied molecular orbital (LUMO) band edges, especially for Pb vacancy and Pb-I antisite surface defects. The passivated perovskite has a smaller band gap than the unpassivated one, which benefits light absorption in the long wavelength range but has no effect on the absorption of visible light, as verified by the ultraviolet-to-visible (UV-vis) absorption spectra [see Fig. 3(b)]. More details about the total density of states for the other three defected structures can be found in Fig. S5 in the Supplemental Material [23].

For perovskite with Pb vacancy defects, there is an interesting change in the electronic property: the perovskite turns from metal to semiconductor after the NPG passivation. Meanwhile, an optical gap is induced, which enhances the absorption of photons over a broad solar spectrum, as shown in Fig. 3(c). In detail, without NPG, the Fermi level is located in the HOMO of the V_{Pb} perovskite surface, indicating that the V_{Pb} perovskite is a metal. On the other hand, the total density of states of the V_{Pb} perovskite passivated by NPG is a simple combination of that of the molecule and the defected perovskite, where the Fermi energy is realigned by the van der Waals interaction between the two [see Fig. 3(d)] [26]. With NPG, the LUMO and the HOMO of V_{Pb} perovskite surface shifts to a lower energy level, and in turn the Fermi level

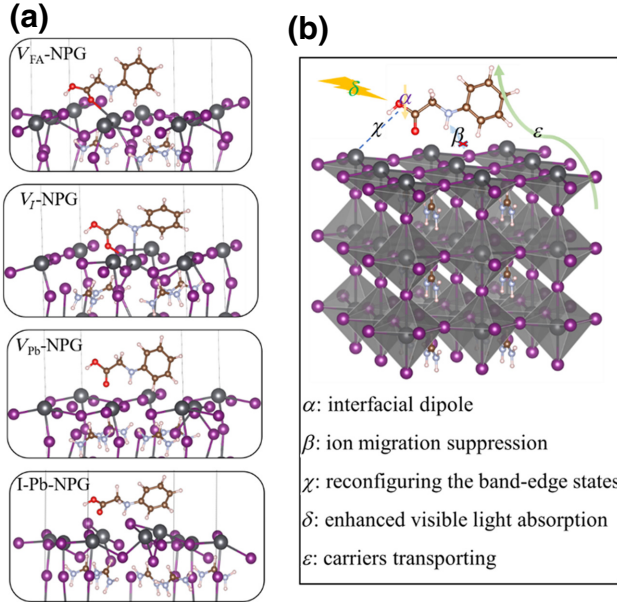


FIG. 2. The optimized interface structures. (a) Interface structures between the surface defects of perovskite films with NPG. (b) Schematic illustrations of the effects of NPG on the perovskite layer.

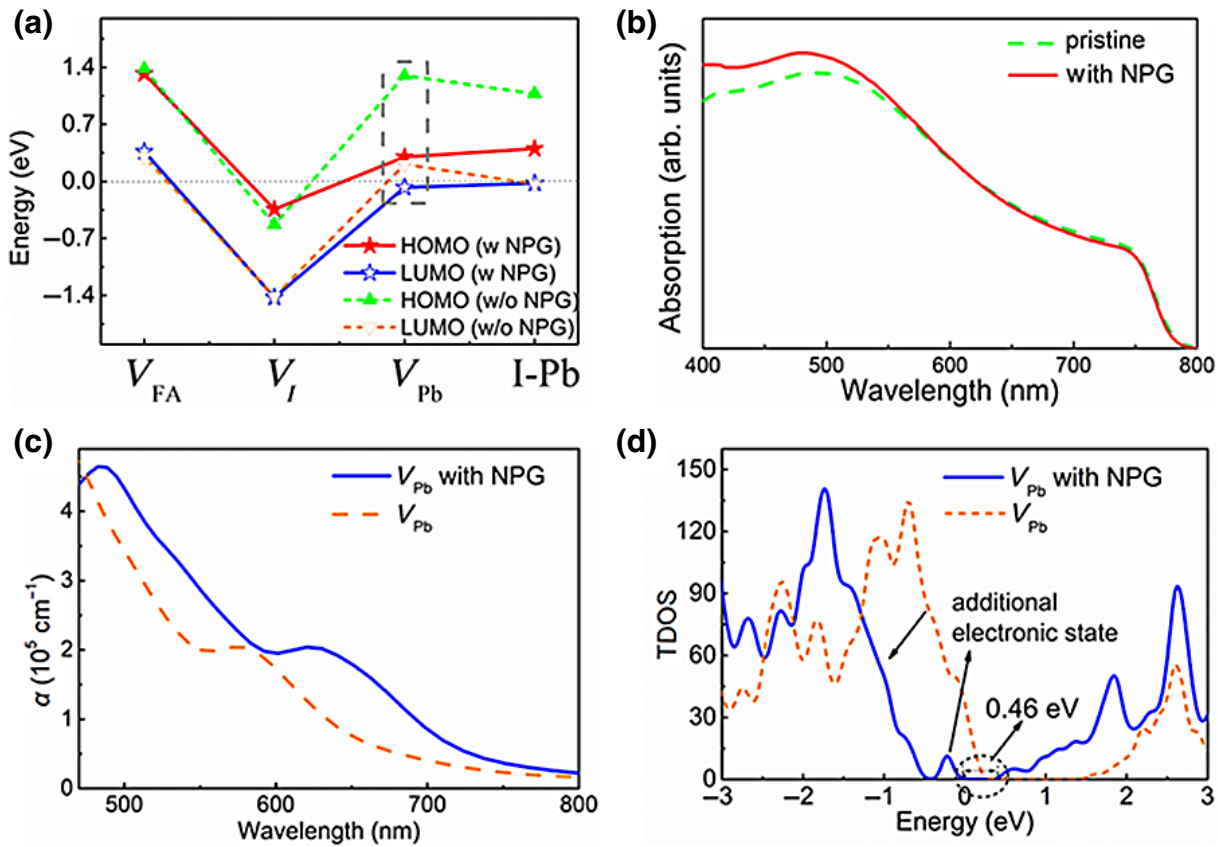


FIG. 3. The optoelectronic properties of pristine and NPG-passivated perovskite. (a) Influences of V_{FA} , V_I , V_{Pb} , and I-Pb on the electronic properties of perovskite. (b) UV-vis spectra of pristine and NPG-passivated perovskite. (c) Visible light absorption coefficient (α) and (d) total density of states (TDOS) of perovskite with V_{Pb} defects, with and without NPG passivation.

lies between the LUMO and the HOMO. One additional electronic state from the NPG molecule appears between the tail of the valence band and the Fermi level. These features support that the V_{Pb} perovskite surface with NPG is a type-II band alignment semiconductor, which provides unique optoelectronic properties that are beneficial to the separation of photogenerated hole-electron pairs and photoconversion applications [27]. As a result, the optoelectronic properties of perovskite can be improved when NPG is introduced to the surface.

To evaluate their potential as high-efficiency PSCs, the electronic properties of the passivated perovskite films are characterized using advanced charge transport characterization techniques. Figure 4(a) shows the Nyquist plots of pristine and NPG-passivated perovskite films, which are measured in the dark and at open-circuit voltages. It can be seen that the series resistance ($R_s = 10 \text{ k}\Omega$) of NPG-passivated perovskite is lower than that of the pristine one ($38 \text{ k}\Omega$). The reduced R_s can slightly increase the fill factor (FF) for the NPG-passivated PSCs. The recombination resistances (R_{rec}) of pristine and NPG-passivated perovskite films are 72.6 and $21.4 \text{ k}\Omega$, respectively. Smaller R_{rec} signifies a stronger depression of charge carrier

recombination. Overall, the perovskite with NPG has smaller charge transfer resistance than the pristine one, suggesting a more efficient charge extraction and transport process for the passivated film.

The steady-state photoluminescence (PL) spectrum [see Fig. 4(b)] shows that the highest PL intensity of perovskite films passivated by NPG is about 4 times larger than that of the pristine films. Thus, the nonradiative recombination loss is alleviated considerably after the surface passivation. The time-resolved PL (TRPL) decay curves [see Fig. 4(c)] are fitted with the biexponential function $I(t) = A_1 \exp(-t/\tau_1) + A_2 \exp(-t/\tau_2)$, where I is the TRPL intensity; A_1 and A_2 are the fast and slow decay amplitude, respectively; t is the TRPL test time of the sample. τ_1 and τ_2 are the fast and slow decay components, respectively [28,29]. The τ_1 of the pristine and the NPG-treated films are 2.40 and 8.71 ns, and the corresponding τ_2 are 128.90 and 176.25 ns. The average lifetimes (τ_{avg}) of the pristine and the NPG-treated films, as calculated by $\tau_{avg} = \sum_{i=1}^n A_i \tau_i^2 / \sum_{i=1}^n A_i \tau_i$, are 138.67 and 156.28 ns, respectively.

Figure 4(d) demonstrates the space-charge-limited current (SCLC) of the pristine and NPG-passivated

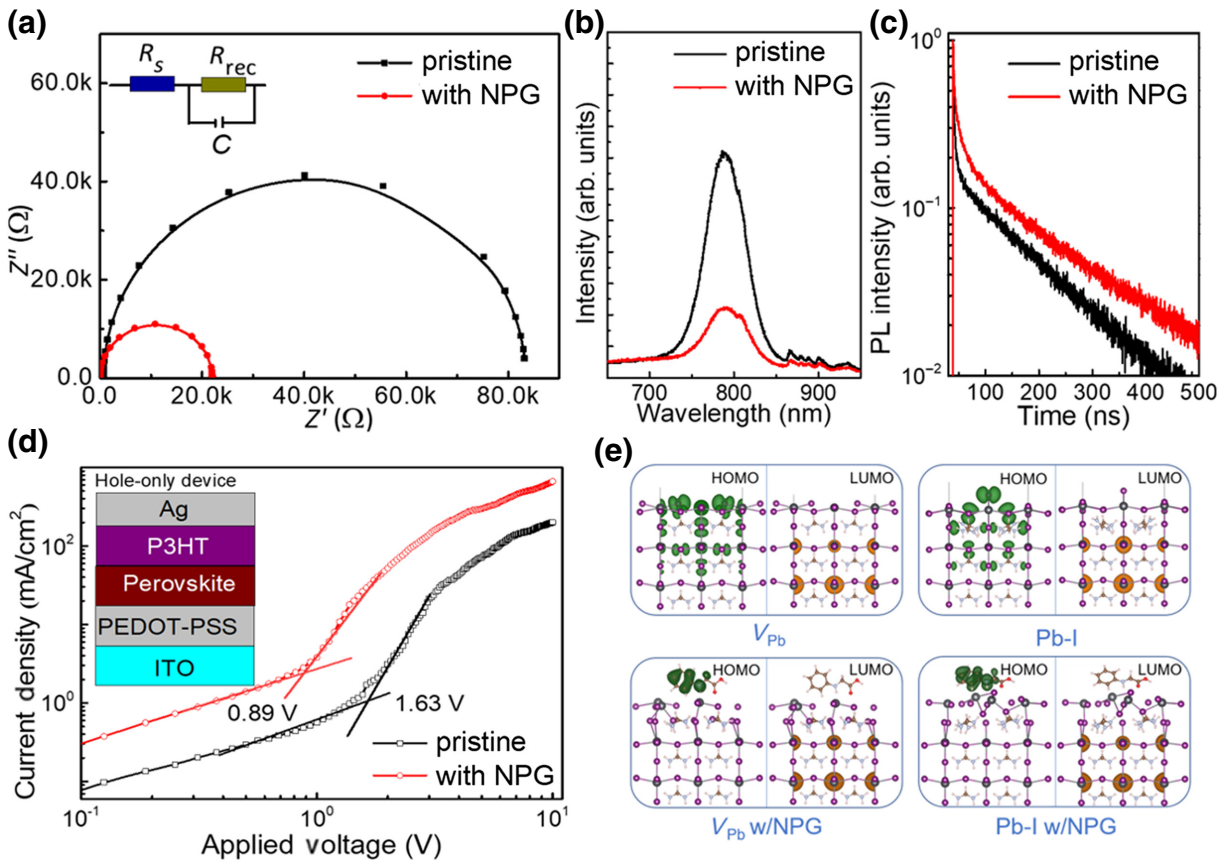


FIG. 4. Performance characterizations of perovskite films. (a) Nyquist plots of pristine and NPG-passivated perovskite films. R_s , series resistance; C , junction capacitance; R_{rec} , recombination resistance. (b) Steady-state PL spectra of pristine and NPG-passivated perovskite films. (c) TRPL spectra of pristine and NPG-passivated perovskite films on TiO_2 /FTO substrates. (d) SCLC of pristine and NPG-passivated perovskite films. P3HT: poly(3-hexylthiophene), PEDOT-PSS: poly(3,4-ethylenedioxythiophene) polystyrene sulfonate, ITO: indium tin oxide. (e) HOMO and LUMO charge densities of the V_{Pb} and I-Pb antisite surface-defected perovskite with and without NPG.

perovskite films, which is a universally used to quantitatively assess the hole mobility (μ_h) and the trap density (N_{trap}) [30]. The μ_h is extracted from fitting the current-voltage curve with the Mott-Gurney equation: $J = (9/8)\mu\epsilon_0\varepsilon(V^2/L^3)$, where μ is the carrier mobility, ε_0 is the permittivity of a vacuum, ε is the dielectric constant of the perovskite, V is the applied voltage, and L is the film thickness. The measured μ_h of NPG-passivated perovskite films ($1.11 \times 10^{-1} \text{ cm}^2 \text{ V}^{-1} \text{ s}^{-1}$) is obviously larger than that of the pristine perovskite films ($4.39 \times 10^{-2} \text{ cm}^2 \text{ V}^{-1} \text{ s}^{-1}$). On the other hand, the N_{trap} value is obtained from the equation $N_{trap} = 2\varepsilon_0\varepsilon V_{TFL}/eL^2$, where V_{TFL} , ε_0 , ε , and e are the trap filled limit voltage, the permittivity of a vacuum, the dielectric constant of the perovskite, and the charge of electron, respectively [31]. From the V_{TFL} value shown in Fig. 4(d), the N_{trap} of the pristine perovskite films is obtained as $3.52 \times 10^{17} \text{ cm}^{-3}$. After the passivation with NPG, N_{trap} deceases to $1.92 \times 10^{17} \text{ cm}^{-3}$. Therefore, the benefits brought by NPG passivation (the increased number of carriers, the longer carrier lifetime, and the enhanced

mobility speed) can promote the photovoltaic performance of the corresponding devices.

The experimental data are supported and explained by the first-principles calculations. Figure 4(e) and Fig. S6 in the Supplemental Material [23] depict the HOMO and LUMO charge densities of the pristine and NPG-passivated perovskite films. The HOMO and LUMO of surface defects display a large overlap of the electron and hole wave functions. The HOMO of the NPG-passivated surfaces moves way from the defect and approaches the NPG molecules, while the LUMO remains in its original location. This explains the more effective hole-electron separation and longer carrier lifetime observed for the NPG-passivated perovskite.

D. Device performance of perovskite solar cells passivated by NPG

Towards the end of our investigation, we discuss the photovoltaic properties of PSCs. First, the corresponding devices are fabricated, with a configuration of FTO

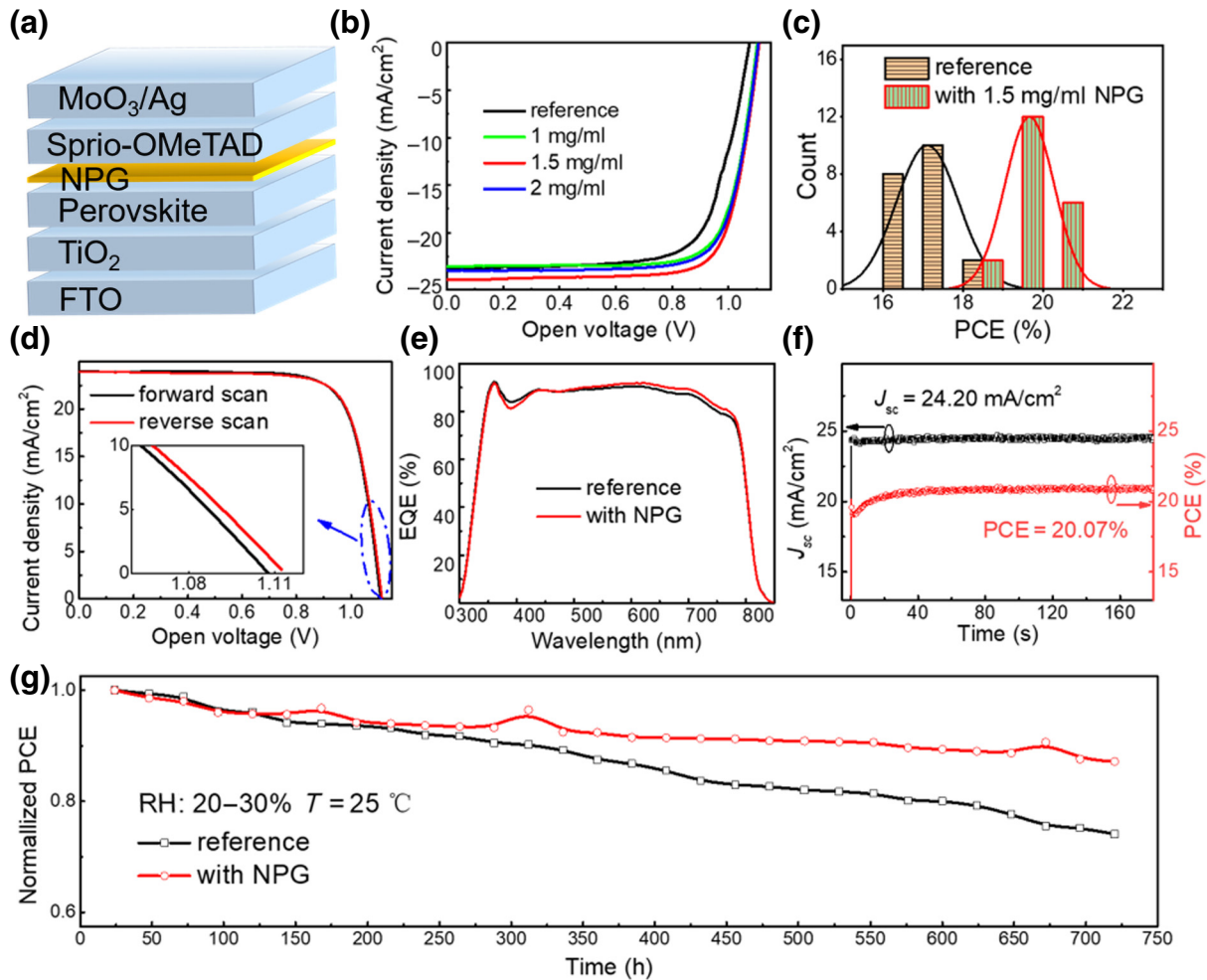


FIG. 5. PSC characterizations. (a) Schematic illustration of fabricated PSCs. (b) J - V curves of PSCs treated by NPG spin coating. (c) PCE distribution of PSCs without and with NPG treatment. (d) J - V curves of forward and reverse scans of PSCs with NPG treatment. (e) EQE curves of PSCs without and with NPG treatment. (f) Stabilized maximum photocurrent density (J) and power output at MPP as a function of time for the best-performing PSCs with NPG treatment, recorded under simulated 1-sun AM1.5G illumination. (g) Evolution of the PCEs measured from the encapsulated PSCs without and with NPG treatment exposed to continuous light ($90 \pm 10 \text{ mW cm}^{-2}$) under open-circuit conditions.

glass/TiO₂/perovskite/NPG/spiro-OMeTAD/MoO₃/Ag, where FTO stands for fluorine-doped tin oxide and spiro-OMeTAD is 2,2',7,7'-Tetrakis[N,N-di(4-methoxyphenyl)lamine]-9,9'-spirobifluorene, [see Fig. 5(a)]. TiO₂ and spiro-OMeTAD are the electron and hole transport layer, respectively. The perovskite layer is made by a typical two-step spin-coating method. The NPG is also spin-coated on perovskite from solutions of different concentrations (1, 1.5, and 2 mg/ml). As shown in the current-density–voltage (J - V) characteristics [see Figs. 5(b) and 5(c) and Table II], The passivated devices show significantly enhanced PCE, and the optimized concentration of NPG for the champion PSCs is 1.5 mg/ml. The champion PSCs show a high PCE of 21.16% (average PCE = 19.71%) with an open-circuit voltage (V_{OC}) of 1.11 V, a short-circuit current density (J_{SC}) of 24.94 mA/cm²,

and a FF of 0.77 under 1-sun illumination (AM1.5G, 100 mW/cm²), which are all higher than those of reference PSCs. The J - V curves of forward and reverse scans of PSCs with NPG are plotted in Fig. 5(d). One can find that the performance of PSCs in the reverse scan is slightly lower than in the forward scan, because PSCs in the reverse scan have a lower V_{OC} .

TABLE II. Device performance parameters of the PSCs.

Device	V_{OC} (V)	J_{SC} (mA/cm ²)	FF	PCE (%)
Reference	1.08	23.76	0.71	18.29
With NPG (1 mg/ml)	1.10	23.56	0.76	19.85
With NPG (1.5 mg/ml)	1.11	24.94	0.77	21.16
With NPG (2 mg/ml)	1.11	23.96	0.76	20.26

The increases in photovoltaic behaviors of NPG-passivated PSCs are confirmed by the external quantum efficiency (EQE) analyses [see Fig. 5(e)]. The integrated photocurrents from EQE spectra are 23.88 and 24.18 mA/cm² for devices without and with 1.5 mg/ml NPG, respectively, agreeing well with the *J-V* measurements (an approximate 3% error). The NPG-passivated PSCs exhibit a higher quantum efficiency in the visible spectral range compared to the reference PSCs. The larger EQE loss in the long wavelength region indicates higher recombination loss in the reference PSCs, causing trapping of low energy photocarriers and reducing the charge extraction from perovskite. The EQE loss in longer wavelengths of reference PSCs is related to the unreacted PbI₂ due to its larger band gap [32]. Figure 5(f) exhibits the stabilized power output at the maximum power point (MPP) for the NPG-treated champion device. The stabilized maximum photocurrent density and stabilized PCE are 24.20 mA cm⁻² and 20.07%, respectively, for the NPG-treated PSCs when biased at 1.00 V. Moreover, the NPG passivation not only enhances the device performance but also improves its stability. The NPG-treated device can maintain over 91% of the initial efficiency while that of the reference device decreases to 75% of its initial efficiency under humid air [relative humidity (RH), 20%–30%, temperature (*T*), 25 °C] and continuous illumination for 700 h [see Fig. 5(g)].

III. CONCLUSIONS

Combining experiments and first-principles simulations, we propose NPG as one universal surface-defect passivant for perovskite to ameliorate photovoltaic performance and stability. The mechanism of interaction between NPG and all typical surface defects of perovskite are analyzed and discussed. The NPG molecules can passivate the organic cation vacancy, I⁻ vacancy, Pb²⁺ vacancy, and Pb-I antisite surface defects of perovskite, through either coordinate and/or hydrogen bonding or the van der Waals interaction. The PSCs passivated by NPG are fabricated, and are shown to have better optoelectronic performance than the reference device. With the introduction of NPG on the perovskite surface, the prepared PSCs have the highest PCE of 21.16% and maintain over 91% of the initial efficiency after 700 h in humid air. Our investigation yields an insight into the interaction mechanisms governing the passivation of perovskite defects, and thus opens one potential route to the design of photovoltaic devices based on perovskite.

ACKNOWLEDGMENTS

Y.N. acknowledges the support of National Natural Science Foundation of China (NSFC) Grant No. 11774294. Computations were conducted in the High-Performance

Computing Center of School of Physical Science and Technology, Southwest Jiaotong University, China.

- [1] R. Siavash Moakhar, S. Gholipour, S. Masudy-Panah, A. Seza, A. Mehdikhani, N. Riahi-Noori, S. Tafazoli, N. Timasi, Y. F. Lim, and M. Saliba, Recent advances in plasmonic perovskite solar cells, *Adv. Sci.* **7**, 1902448 (2020).
- [2] Z. Xiao, R. A. Kerner, L. Zhao, N. L. Tran, K. M. Lee, T.-W. Koh, G. D. Scholes, and B. P. Rand, Efficient perovskite light-emitting diodes featuring nanometre-sized crystallites, *Nat. Photonics* **11**, 108 (2017).
- [3] A. Miyata, A. Mitioglu, P. Plochocka, O. Portugall, J. T.-W. Wang, S. D. Stranks, H. J. Snaith, and R. J. Nicholas, Direct measurement of the exciton binding energy and effective masses for charge carriers in organic-inorganic tri-halide perovskites, *Nat. Phys.* **11**, 582 (2015).
- [4] S. P. Senanayak, B. Yang, T. H. Thomas, N. Giesbrecht, W. Huang, E. Gann, B. Nair, K. Goedel, S. Guha, and X. Moya, Understanding charge transport in lead iodide perovskite thin-film field-effect transistors, *Sci. Adv.* **3**, e1601935 (2017).
- [5] W. Zhang, G. E. Eperon, and H. J. Snaith, Metal halide perovskites for energy applications, *Nat. Energy* **1**, 1 (2016).
- [6] H. Keppler, L. S. Dubrovinsky, O. Narygina, and I. Kantor, Optical absorption and radiative thermal conductivity of silicate perovskite to 125 gigapascals, *Science* **322**, 1529 (2008).
- [7] E. Oksenberg, A. Merdasa, L. Houben, I. Kaplan-Ashiri, A. Rothman, I. G. Scheblykin, E. L. Unger, and E. Joselevich, Large lattice distortions and size-dependent bandgap modulation in epitaxial halide perovskite nanowires, *Nat. Commun.* **11**, 1 (2020).
- [8] S. Shao and M. A. Loi, Advances and prospective in metal halide ruddlesden-popper perovskite solar cells, *Adv. Energy Mater.* **11**, 2003907 (2021).
- [9] N. Y. Nia, D. Saranin, A. L. Palma, and A. Di Carlo, *Perovskite Solar Cells, Solar Cells and Light Management* (Elsevier, Venice, 2020), pp. 163–228.
- [10] W.-Q. Wu, Z. Yang, P. N. Rudd, Y. Shao, X. Dai, H. Wei, J. Zhao, Y. Fang, Q. Wang, and Y. Liu, Bilateral alkylamine for suppressing charge recombination and improving stability in blade-coated perovskite solar cells, *Sci. Adv.* **5**, eaav8925 (2019).
- [11] D. Meggiolaro, E. Mosconi, and F. De Angelis, Formation of surface defects dominates ion migration in lead-halide perovskites, *ACS Energy Lett.* **4**, 779 (2019).
- [12] W. Ouyang, F. Teng, J. H. He, and X. Fang, Enhancing the photoelectric performance of photodetectors based on metal oxide semiconductors by charge-carrier engineering, *Adv. Funct. Mater.* **29**, 1807672 (2019).
- [13] A. N. Singh, S. Kajal, J. Kim, A. Jana, J. Y. Kim, and K. S. Kim, Interface engineering driven stabilization of halide perovskites against moisture, heat, and light for optoelectronic applications, *Adv. Energy Mater.* **10**, 2000768 (2020).

- [14] J. Jeong, M. Kim, J. Seo, H. Lu, P. Ahlawat, A. Mishra, Y. Yang, M. A. Hope, F. T. Eickemeyer, and M. Kim, Pseudo-halide anion engineering for α -FAPbI₃ perovskite solar cells, *Nature* **592**, 381 (2021).
- [15] F. Zhang and K. Zhu, Additive engineering for efficient and stable perovskite solar cells, *Adv. Energy Mater.* **10**, 1902579 (2020).
- [16] H. Zhang, Z. Chen, M. Qin, Z. Ren, K. Liu, J. Huang, D. Shen, Z. Wu, Y. Zhang, and J. Hao, Multifunctional crosslinking-enabled strain-regulating crystallization for stable, efficient α -FAPbI₃-based perovskite solar cells, *Adv. Mater.* **33**, 2008487 (2021).
- [17] K. Wang, J. Liu, J. Yin, E. Aydin, G. T. Harrison, W. Liu, S. Chen, O. F. Mohammed, and S. De Wolf, Defect passivation in perovskite solar cells by cyano-based π -conjugated molecules for improved performance and stability, *Adv. Funct. Mater.* **30**, 2002861 (2020).
- [18] R. Wang, J. Xue, K.-L. Wang, Z.-K. Wang, Y. Luo, D. Fenning, G. Xu, S. Nuryyeva, T. Huang, and Y. Zhao, Constructive molecular configurations for surface-defect passivation of perovskite photovoltaics, *Science* **366**, 1509 (2019).
- [19] B. Wenger, P. K. Nayak, X. Wen, S. V. Kesava, N. K. Noel, and H. J. Snaith, Consolidation of the optoelectronic properties of CH₃NH₃PbBr₃ perovskite single crystals, *Nat. Commun.* **8**, 1 (2017).
- [20] A. J. Cohen, P. Mori-Sánchez, and W. Yang, Insights into current limitations of density functional theory, *Science* **321**, 792 (2008).
- [21] D. Zhang, S. Hu, X. Liu, Y. Chen, Y. Xia, H. Wang, H. Wang, and Y. Ni, Solar cells based on Two-dimensional WTe₂/PtXY(X, Y = S, Se) heterostructures with high photoelectric conversion efficiency and Low power consumption, *ACS Appl. Energy Mater.* **4**, 357 (2020).
- [22] D. Zhang, Y. Hu, H. Zhong, S. Yuan, and C. Liu, Effects of out-of-plane strains and electric fields on the electronic structures of graphene/MTe (M = Al, B) heterostructures, *Nanoscale* **11**, 13800 (2019).
- [23] See the Supplemental Material at <http://link.aps.org/supplemental/10.1103/PhysRevApplied.17.024039> for more information about materials, device fabrication, characterization, and calculation methods.
- [24] S. Masi, A. F. Gualdrón-Reyes, and I. Mora-Sero, Stabilization of black perovskite phase in FAPbI₃ and CsPbI₃, *ACS Energy Lett.* **5**, 1974 (2020).
- [25] P. Liu, N. Han, W. Wang, R. Ran, W. Zhou, and Z. Shao, High-Quality ruddlesden–popper perovskite film formation for high-performance perovskite solar cells, *Adv. Mater.* **33**, 2002582 (2021).
- [26] D. Zhang, Q. Gao, Y. Chen, Y. Xia, H. Wang, H. Wang, and Y. Ni, Tunable electronic properties and potential applications of BSe/XS₂ (X = Mo, W) van der waals heterostructures, *Adv. Theory Simul.* **3**, 2000144 (2020).
- [27] M.-H. Chiu, C. Zhang, H.-W. Shiu, C.-P. Chuu, C.-H. Chen, C.-Y. S. Chang, C.-H. Chen, M.-Y. Chou, C.-K. Shih, and L.-J. Li, Determination of band alignment in the single-layer MoS₂/WSe₂ heterojunction, *Nat. Commun.* **6**, 1 (2015).
- [28] Z. Gan, X. Wen, C. Zhou, W. Chen, F. Zheng, S. Yang, J. A. Davis, P. C. Tapping, T. W. Kee, and H. Zhang, Transient energy reservoir in 2D perovskites, *Adv. Opt. Mater.* **7**, 1900971 (2019).
- [29] P. Chen, Y. Bai, S. Wang, M. Lyu, J. H. Yun, and L. Wang, In situ growth of 2D perovskite capping layer for stable and efficient perovskite solar cells, *Adv. Funct. Mater.* **28**, 1706923 (2018).
- [30] V. M. Le Corre, E. A. Duijnsteene, O. El Tambouli, J. M. Ball, H. J. Snaith, J. Lim, and L. J. A. Koster, Revealing charge carrier mobility and defect densities in metal halide perovskites via space-charge-limited current measurements, *ACS Energy Lett.* **6**, 1087 (2021).
- [31] H. Li, L. Duan, D. Zhang, and Y. Qiu, Electric field inside a hole-only device and insights into space-charge-limited current measurement for organic semiconductors, *J. Phys. Chem. C* **118**, 9990 (2014).
- [32] S. D. Stranks, Nonradiative losses in metal halide perovskites, *ACS Energy Lett.* **2**, 1515 (2017).